J. Fluid Mech. (1980), *vol.* 96, *part* 1, *pp.* 27–32
Printed in Great Britain

On flow through furrowed channels. Part 2. Observed flow patterns

By K. D. STEPHANOFF, IAN J. SOBEY AND B. J. BELLHOUSE
Department of Engineering Science, Oxford University

(Received 22 December 1978)

Observations of flow in furrowed channels support the calculations of part 1 (Sobey 1980). If the mainstream flow is steady there is a critical Reynolds number below which separation does not occur. Above that Reynolds number vortices form and fill the furrow. When the mainstream is oscillatory, the flow may separate during the acceleration to form strong vortices. During the deceleration the vortices grow to fill the furrow and channel. As the mainstream reverses the vortices are ejected from the furrows as the fluid flows between the wall and the vortex. Photographs show that this pattern occurs for sinusoidally varying walls, furrows that are arcs of circles and rectangular hollows.

1. Introduction

In part 1 (Sobey 1980) numerical solutions to the Navier–Stokes equations of motion have shown the complex structure of steady and unsteady flow through a two-dimensional symmetrically furrowed channel. The numerical solutions have shown that for steady flow there is a critical Reynolds number below which separation does not occur. As the Reynolds number increases above the critical value a vortex is set up in the furrows of the channel wall. The vortex rapidly grows with increasing Reynolds number until it is centred in the downstream part of the furrow and fills the furrow. In unsteady flow the situation is much more complex. There are two parameters which govern the flow: (1) the pulsatile Reynolds number,

$$\alpha^2 = h^2\Omega/\nu,$$

where h is the channel half-gap, Ω the frequency of oscillation and ν the kinematic viscosity; and (2) the Strouhal number,

$$St = \Omega h/U,$$

where U is the peak velocity obtained by assuming a flat velocity profile. At small Strouhal numbers (of the order 10^{-2}) the flow develops in a quasi-steady manner during the acceleration and, provided the peak instantaneous Reynolds number

$$Re = \alpha^2/St$$

is greater than the critical Reynolds number for steady flow separation, the oscillatory flow will separatc causing a vortex to form in the furrow. A major feature of the numerical solution concerns the development of the vortex during the deceleration.

0022-1120/80/4347-7900 $02.00

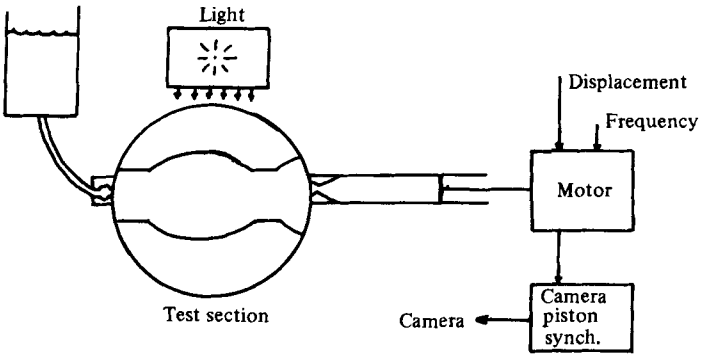

FIGURE 1. Schematic layout of experimental rigs.

Sobey (1980) predicts that the vortex will expand during a deceleration, in contradiction to quasi-steady ideas. The expansion is followed by ejection of the vortex from the furrow as the reversing fluid flows between the vortex and the wall. In this paper we support the numerical results by demonstrating visually the process of vortex formation, growth and subsequent ejection from a furrow. The observations were made in small tunnels using polystyrene particles to show the flow paths.

2. Experimental details

Two small rigs were used to observe flow through furrowed channels. A schematic diagram is shown in figure 1. The test sections used were sinusoidally shaped walls, furrows that were arcs of circles and rectangular furrows. The test sections were machined from Perspex. As discussed in part 1, the particular application we are interested in is the high efficiency membrane oxygenator of Bellhouse *et al.* (1973), where the furrows are arcs of circles and the scale is very small, channel half-gap 0·025 cm, hollow chord 0·2 cm and hollow depth 0·05 cm. Experimentally it is simpler to scale the geometry up but in unsteady flow this procedure is not as useful as in steady flow. There are *two* governing parameters, the Reynolds number and the Strouhal number, and in order to have similar flows both parameters must be kept constant. If the scale is increased the velocity scale must decrease to preserve the Reynolds number and then the frequency must decrease by the *square* of the scale factor to keep the Strouhal number constant. In order to avoid very small operating frequencies we have used a scale of approximately twice that given for the oxygenator. To observe flows on this small scale we have used polystyrene particles of diameter 15–125 μm and have accepted that some errors will be introduced by using particles with diameters between $\frac{1}{10}$ and $\frac{1}{20}$ the minimum channel gap.

The use of such relatively large particles has allowed a cheap light source to be used, a 150 W slide projector with a quartz halogen bulb. Still photographs were taken using Kodak 2475 recording film and exposure times down to $\frac{1}{125}$ s at $f3{\cdot}5$. Synchronization of the photographs with the piston motion was achieved by using a camera with an electronic shutter (Nikon F2 body with MDZ motor drive and micro-Nikkor 55 mm lens). There was a constant delay of 75 ms between the trigger pulse and the camera firing. On one rig both the frequency and displacement of the piston could be continuously set and on the other rig only the frequency. However on the latter rig the

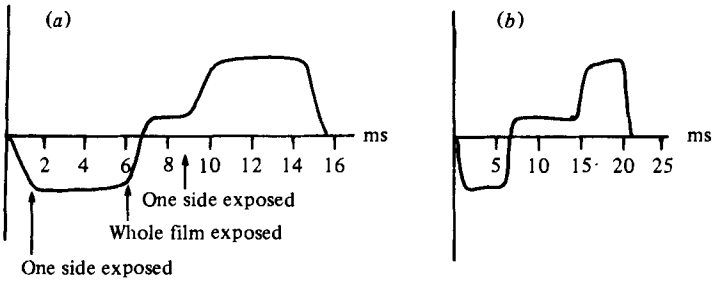

FIGURE 2. Traces obtained by subtracting the output of two light-sensitive transistors to measure camera blind movement (*a*) $\frac{1}{125}$ second, (*b*) $\frac{1}{60}$ second.

piston motion more closely resembled a sine wave than on the other. The camera could be set to fire at 10 ms points during a cycle with an accuracy of 1 μs. There are many difficulties in still photography of continuous events. One difficulty is the exposure of one side of the film before the other side as the shutter blinds move across the film. To demonstrate this difficulty we used two light-sensitive transistors placed in the position of the film behind the exposure window. The output from the two transistors was subtracted and typical traces are shown in figure 2. It can be seen that the blind takes approximately $\frac{1}{100}$ s to traverse the film. At $\frac{1}{125}$ s the whole film is exposed for only a few milliseconds (figure 2*a*) whilst at $\frac{1}{60}$ s the situation is somewhat better, the whole film is exposed for nearly 10 ms (figure 2*b*). The time of exposure was also measured and we found that the camera was very reliable, giving exposure times of 14·5 ms at $\frac{1}{60}$ s, 12·5 ms at $\frac{1}{80}$ s and 8·5 ms at $\frac{1}{125}$ s. Knowing these times and by measuring the particle paths on the film it is hoped to obtain velocity profiles at a later stage.

We have indicated that there will be several sources of error at our work:

(1) the relatively large particle sizes,
(2) deviation of the piston stroke from sinusoidal motion,
(3) inaccuracies introduced by the nature of still photography.

It is difficult to quantify these errors in unsteady motion. We have attempted to minimize them and as we are presenting qualitative results we feel justified in neglecting the magnitude of these errors at this stage.

3. Steady flow

In part 1 it was shown that there is a critical Reynolds number below which steady flow does not separate. Define the hollow length to be Lh and depth Dh, where h is the channel half-gap. For a sinusoidal hollow of length $L = 8$ and depth $D = 2$ the critical Reynolds number is near 5. In figure 3 (plate 1) we show photographs of steady flow for furrows of non-dimensional length $L = 15$ and depth $D = 4$. Using § 5.2 of part 1 we can deduce that the effect of increasing the scale of the furrows to $L = 15$ and $D = 4$ is to reduce slightly the critical Reynolds number. In the photographs the mainstream is moving from right to left. Figure 3 (*a*) shows that at $Re = 5{\cdot}3$ there is a considerable stagnant region in the upstream part of the furrow. It is difficult to determine whether separation has occurred because the particles move very slowly and are not displaced

a great distance during the time of the photograph. At Reynolds number of 8·9 (figure 3*b*) the stagnant region has increased in size and a slowly rotating vortex was visible. At a Reynolds number of 15·5 (figure 3*c*) the characteristic vortex motion can be seen in the photograph. In figure 3(*d*) the flow is shown at $Re = 28{\cdot}9$. The vortex fills the furrow and during the exposure of the photograph particles in the furrow move a considerable distance. The features shown in these photographs are consistent with the numerical studies of part 1, in particular the occurrence of separation near $Re = 5$ and the rapid growth of the vortex to fill the furrow as the Reynolds number increases to near 30.

4. Unsteady flow

In the calculations presented in part 1 there were several major points that we shall reiterate here before discussing the photographs shown in figures 4–9 (plates 2–7). Firstly it was shown that during a deceleration the vortex would grow in size although not in strength. Even though the flow appeared to behave during the acceleration in a quasi-steady manner the behaviour during the deceleration was in complete contradiction to quasi-steady theory. Secondly it was shown in part 1 that the geometric parameters of most importance were the hollow length and depth. Details of the wall geometry, such as the presence of corners, seemed to have little influence on the flow patterns calculated in the furrowed channels. Lastly, using the definitions of part 1, if the time of separation is taken as a global parameter, then in terms of the pulsatile Reynolds number and the Strouhal number a singularity develops near the origin. The angle the singularity makes with the origin corresponds to the critical Reynolds number for separation of steady flow through a furrowed channel. It is important to understand that the structure of the solutions presented in part 1 should be true for oscillatory flow through furrows of arbitrary geometry.

In figure 4 (plate 2) we show the development of the vortex in a sinusoidally varying channel as the flow decelerates. The Reynolds number is 32·5 and it can be seen that late in the half-cycle (figure 4*a*) the vortex remains entirely within the furrow. At a non-dimensional time, $t = 0{\cdot}925$ (figure 4*b*), the vortex has bulged into the mainstream. One effect of this is to keep the velocity in the centre of the mainstream nearly constant as the flow decelerates. At $t = 0{\cdot}956$ (figure 4*c*) the vortex has continued to expand and occupies much of the mainstream. In figure 4(*d*), taken at $t = 0{\cdot}994$, the vortex has grown to fill the furrow and the channel. Fluid is flowing back along the wall and forward in the centre of the channel.

In figure 5 (plate 3) we show the movement of the vortex after the flow has reversed. At $t = 0{\cdot}004$ the vortex fills the furrow and the channel and as the flow reverses the fluid flows between the vortex and the wall, displacing the vortex into the mainstream. As the flow accelerates in the opposite direction fluid from the vortex is gathered into the mainstream reducing the size of the vortex (figure 5*b–e*). Continued acceleration removes the vortex altogether and at $t = 0{\cdot}12$ the fluid is flowing through the furrow mainly following the wall shape. It can be seen that the ejection of the vortex from the furrow and the subsequent elimination of the displaced vortex in the mainstream is a very rapid process that occurs when the mainstream flow reverses direction.

To demonstrate that the flow structure remains unaltered with changing geometry we show in figures 6–9 photographs taken in widely varying situations. In figure 6

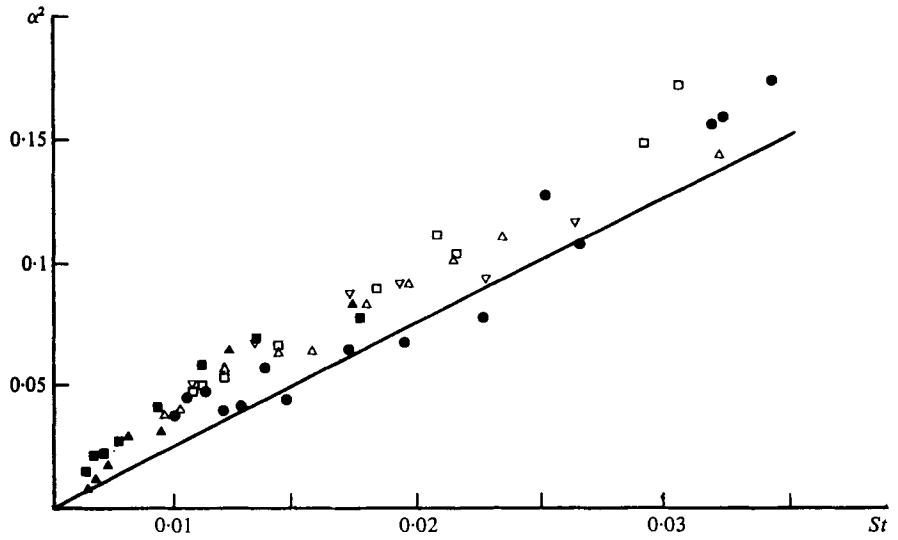

FIGURE 10. Observations of the onset of vortex formation in a sinusoidally furrowed channel. ● = 0·01S, △ = 0·0567S, □ = 0·0737S, ▽ = 0·0987S, ■ = 0·0957S (half-scale model) ▲ = 0·098S (half-scale model). —— calculated line dividing those flows that separate in the acceleration (above the line) from those that separate in the deceleration.

(plate 4) the furrows are semicircles. As the flow reverses the vortex is displaced into the mainstream (figure 6a) and eventually separation occurs in the upstream part of the furrow (figure 6b). The old pair of vortices still remain in the centre of the channel, although of greatly diminished size. Further acceleration of the mainstream increases the size of the separated region (figure 6c) and at peak flow the vortex fills the furrow (figure 6d). As the flow decelerates the vortex bulges into the mainstream (figure 6e) and when the flow finally comes to rest the vortex is left rotating in the hollow and mainstream (figure 6f).

If we consider a rectangular hollow the situation remains unaltered. In order to stress this we show the flow in a one-sided furrow; the upper wall in the photographs is a flat wall. In figure 7 (a) (plate 5) the vortex from the previous half-cycle can be seen in the hollow. As the fluid begins to move it is clear from figure 7 (b) that the old vortex has been displaced to a position near the upper wall, the flow has separated from the upstream wall and the mainstream flows between the vortices. In figures 7 (c) and (d) the continued growth of the new vortex is shown together with the final elimination of the old vortex. During the cycle the vortex moves into the downstream part of the hollow and the fluid in the upstream part becomes stagnant (figure 7e, f). As the mainstream decelerates to rest the vortex increases in size (figure 7g) and finally occupies the channel and the hollow (figure 7h). An increase in the hollow depth has little effect on the structure of the flow cycle. In figures 8 (a) and 9 (a) (plates 6 and 7) the vortex from the previous half-cycle can be seen rotating in the hollow, filling the hollow and the mainstream. As the fluid is accelerated the vortex is displaced from the hollow. The new vortex moves across the hollow and eventually grows in size as the mainstream decelerates. This pattern is evident in both figures 8 and 9.

We have observed visually in sinusoidal furrows the onset of vortex motion on a yes/no basis. In figure 10 we show the results for varying viscosity and hollow scale.

A consistent pattern emerges, vortices only being observed if the peak Reynolds number is sufficiently great. We also show the calculated line (from part 1) that divides those flows which separate in accelerating flow from those that separate in decelerating flow. These observations support the conclusions of part 1 that the flow develops in a quasi-steady manner during the acceleration phase and that vortices will be observed only if the peak Reynolds number is greater than some critical value, the critical value being that Reynolds number that would cause a steady flow to separate. This is, of course, a valuable design criterion as well as a link in our picture of the structure of unsteady fluid flows.

We are grateful to F. H. Bellhouse, M. Stevenson and J. Mooney for technical assistance, and to R. D. Hill for design and construction of the piston/camera synchronization unit. This work is supported by the Science Research Council. K. D. S. gratefully acknowledges receipt of a Thouron Scholarship from the University of Pennsylvania.

REFERENCES

BELLHOUSE, B. J., BELLHOUSE, F. H., CURL, C. M., MACMILLAN, T. I., GUNNING, A. J., SPRATT, E. H., MACMURRAY, S. B. & NELEMS, J. M. 1973 A high efficiency membrane oxygenator and pulsatile pumping system, and its application to animal trials. *Trans. Amer. Soc. Artif. Int. Organs* **19**, 72–79.

SOBEY, I. J. 1980 On flow through furrowed channels. Part 1. Calculated flow patterns. *J. Fluid Mech.* **96**, 1–36.

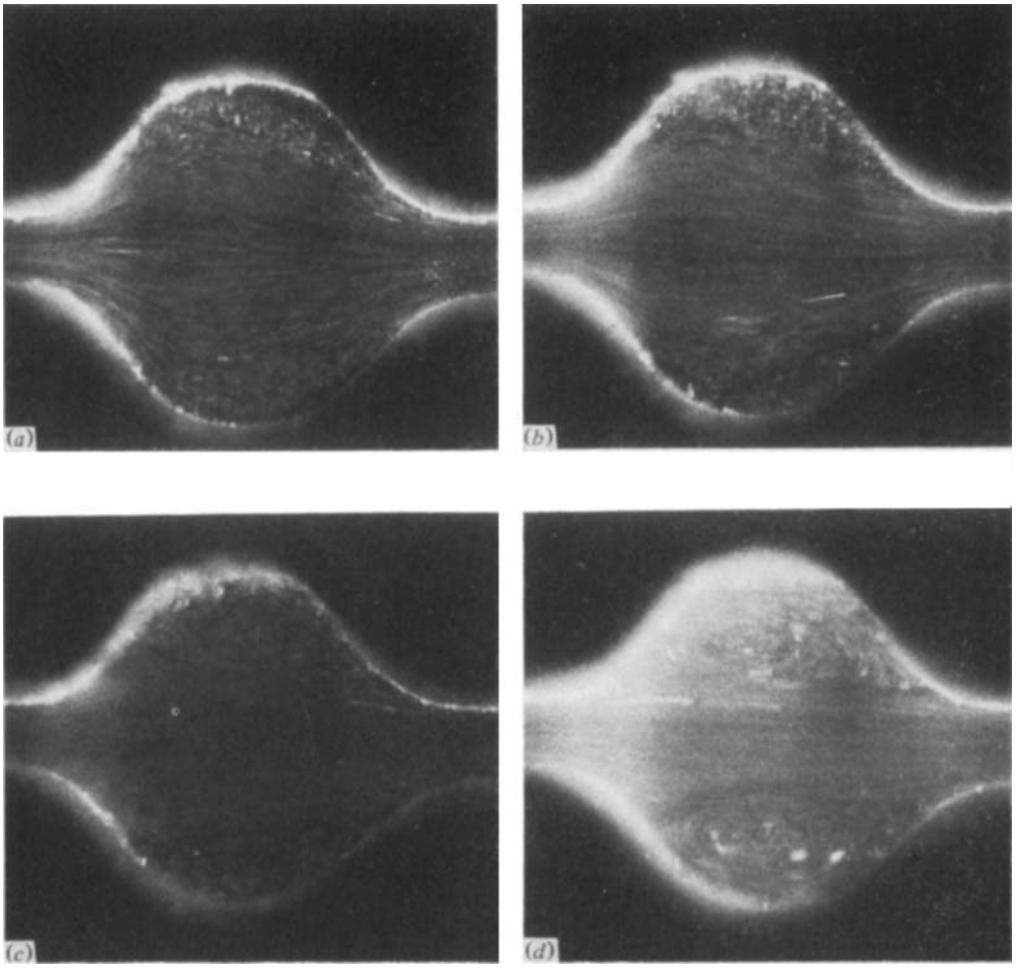

FIGURE 3. Steady flow through a sinusoidal furrow. (*a*) $Re = 5{\cdot}3$, (*b*) $Re = 8{\cdot}9$, (*c*) $Re = 15{\cdot}5$, (*d*) $Re = 28{\cdot}9$. Hollow dimensions $h = 0{\cdot}04$ cm, $L = 15$, $D = 4$.

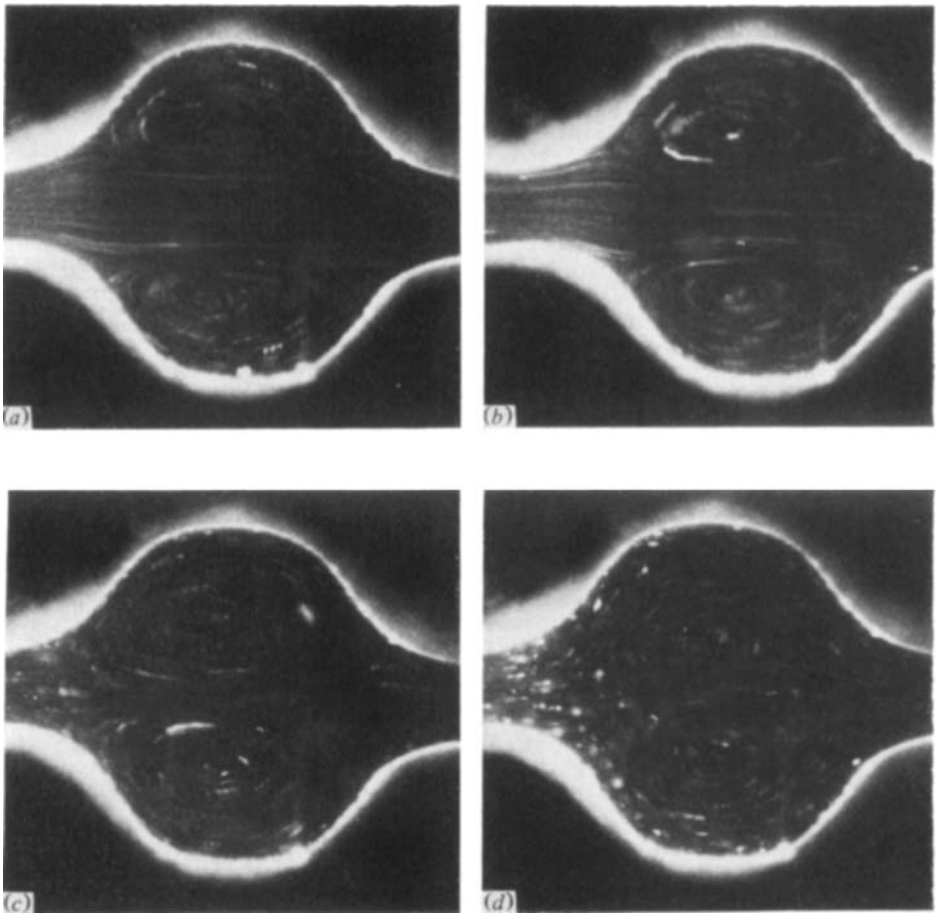

FIGURE 4. Growth of vortices during final stages of deceleration. (*a*) $t = 0{\cdot}894$, (*b*) $t = 0{\cdot}925$, (*c*) $t = 0{\cdot}956$, (*d*) $t = 0{\cdot}994$. Pulsatile Reynolds number = 0·156, Strouhal number = 0·0048. Furrow dimensions as in figure 3.

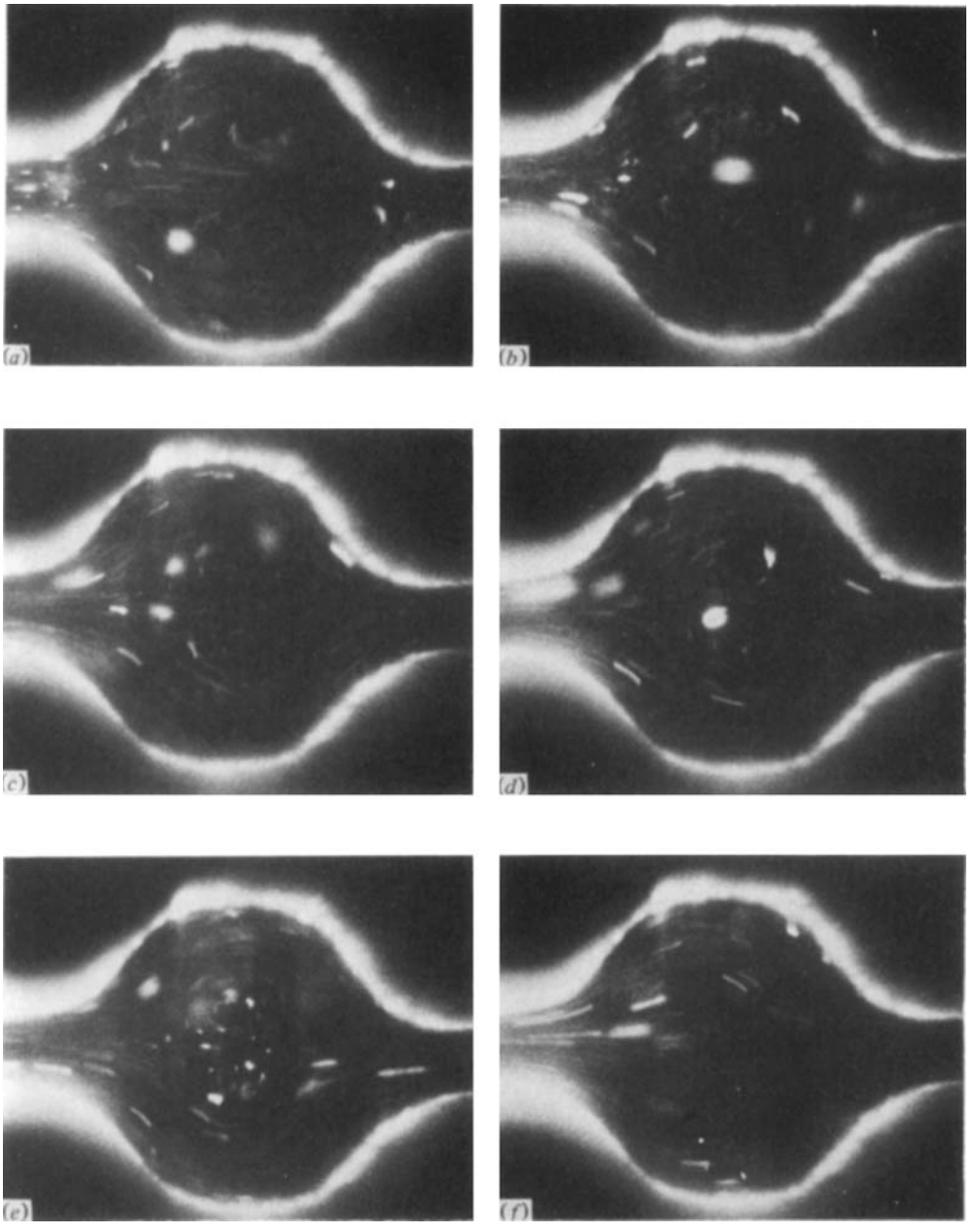

FIGURE 5. Elimination of vortices after ejection from furrows. (*a*) $t = 0{\cdot}004$, (*b*) $t = 0{\cdot}015$, (*c*) $t = 0{\cdot}030$, (*d*) $t = 0{\cdot}045$, (*e*) $t = 0{\cdot}075$, (*f*) $t = 0{\cdot}12$. Pulsatile Reynolds number = 0·375 and Strouhal number = 0·0048. Furrow dimensions as in figure 3.

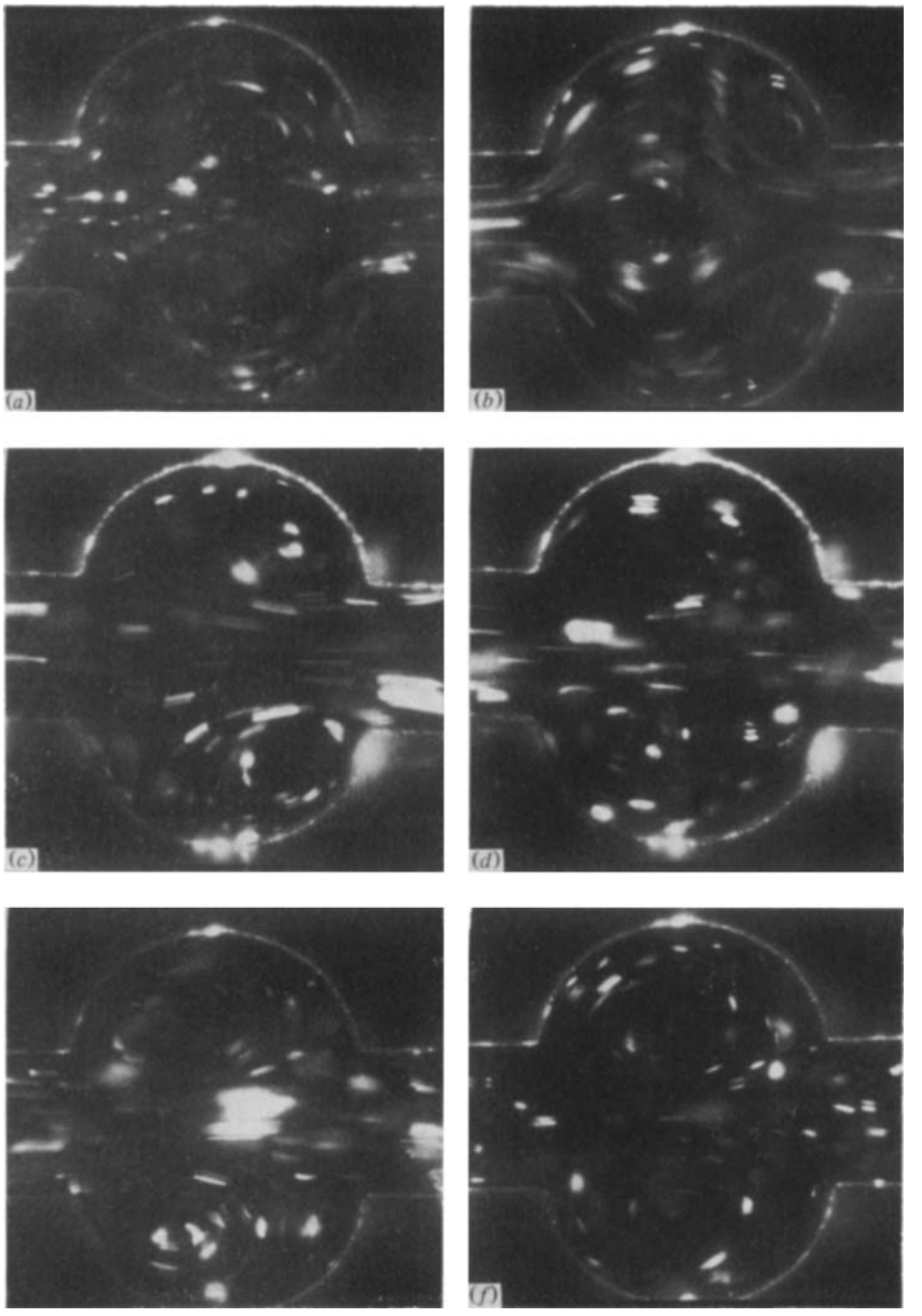

FIGURE 6. Flow cycle for semicircular furrow. (*a*) $t = 0{\cdot}01$, (*b*) $t = 0{\cdot}18$, (*c*) $t = 0{\cdot}23$, (*d*) $t = 0{\cdot}35$, (*e*) $t = 0{\cdot}48$, (*f*) $t = 0{\cdot}60$. Pulsatile Reynolds number = 0·25, Strouhal number 0·003. Hollow dimensions $h = 0{\cdot}1$ cm, $L = 4$ and $D = 2$.

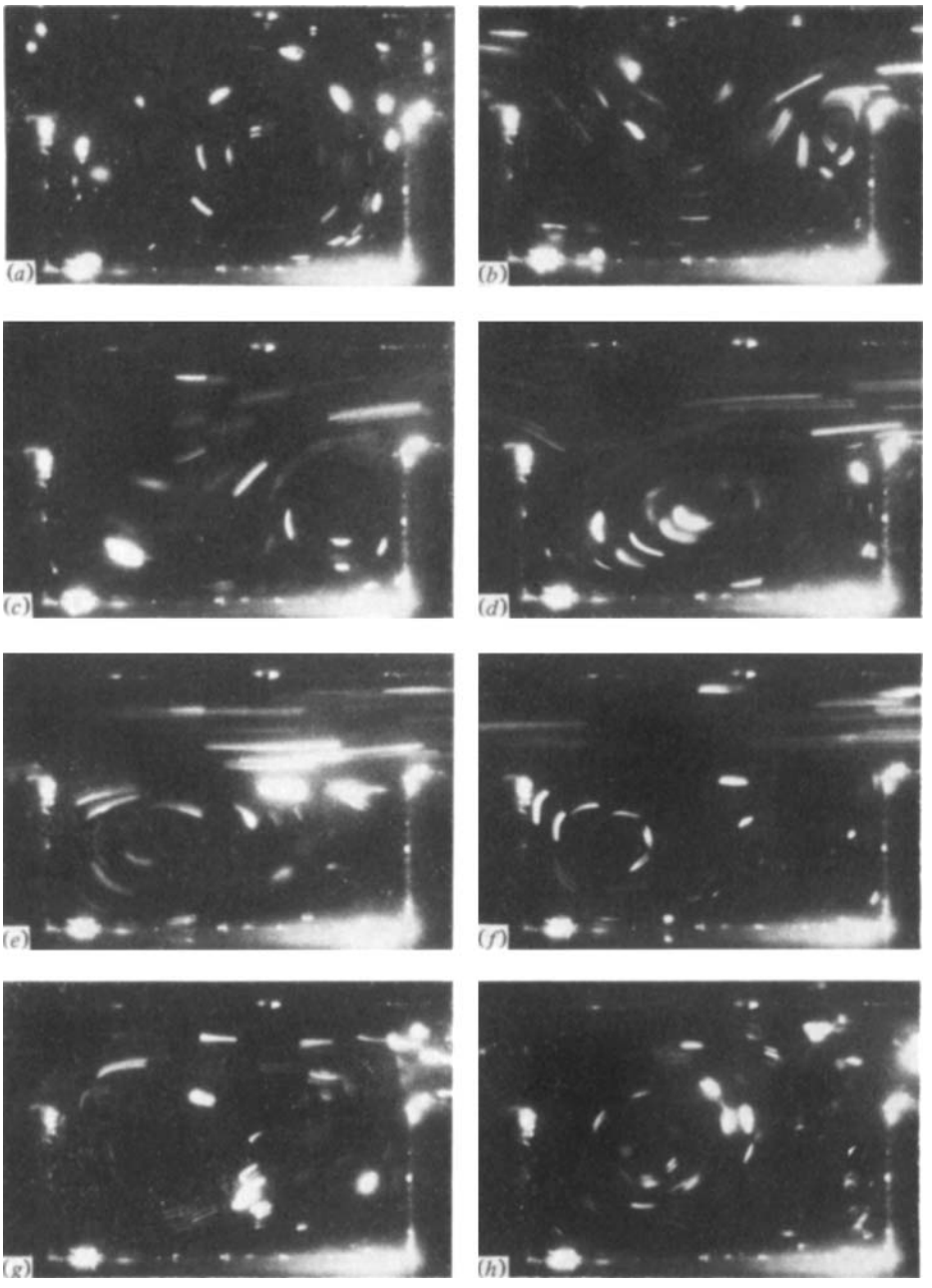

Figure 7. Flow cycle for rectangular hollow. (*a*) $t = 0{\cdot}08$; (*b*) $t = 0{\cdot}12$; (*c*) $t = 0{\cdot}15$; (*d*) $t = 0{\cdot}19$; (*e*) $t = 0{\cdot}23$; (*f*) $t = 0{\cdot}36$; (*g*) $t = 0{\cdot}44$; (*h*) $t = 0{\cdot}53$. Pulsatile Reynolds number = 0·21, Strouhal number = 0·0031. Hollow dimensions $h = 0{\cdot}05$ cm, $L = 10$, $D = 4$.

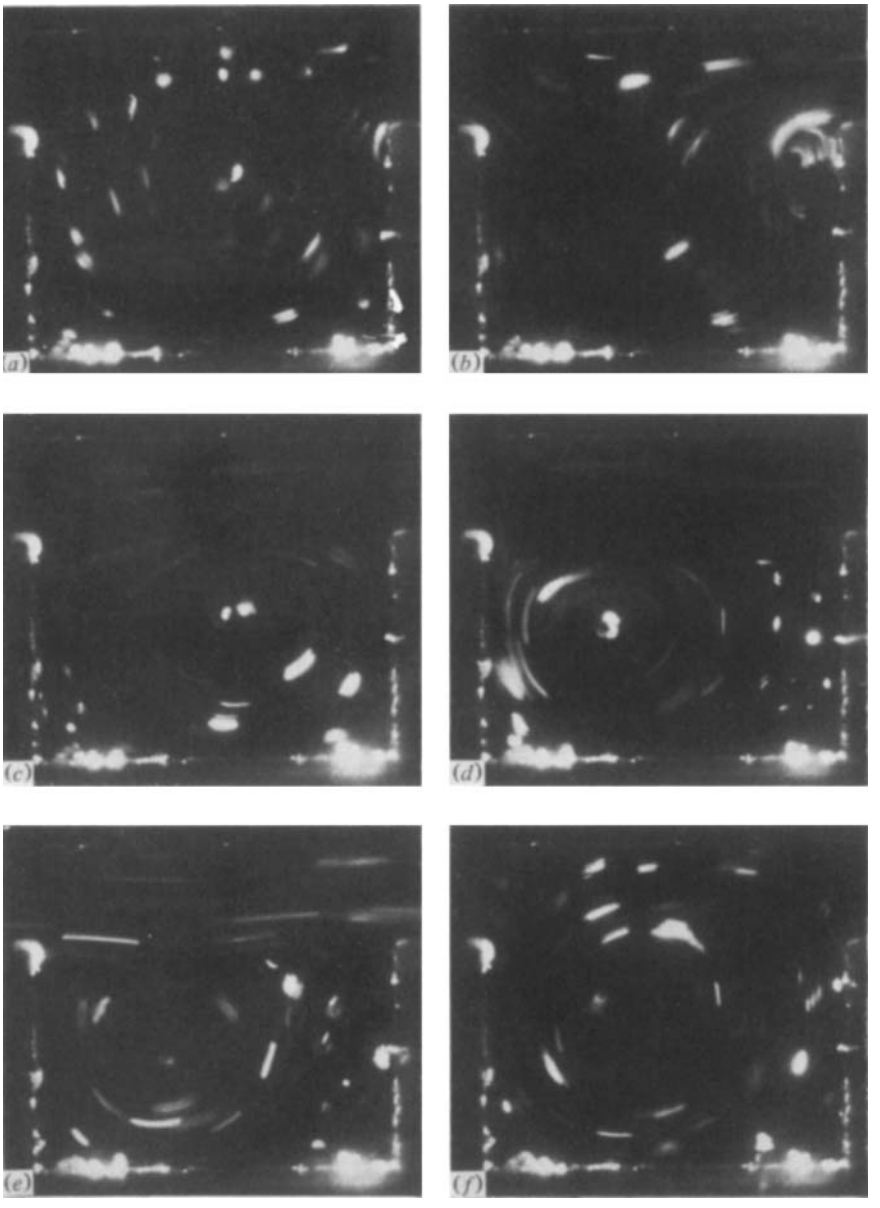

FIGURE 8. Flow cycle for rectangular hollow. (*a*) $t = 0{\cdot}12$; (*b*) $t = 0{\cdot}13$, (*c*) $t = 0{\cdot}19$; (*d*) $t = 0{\cdot}23$; (*e*) $t = 0{\cdot}25$; (*f*) $t = 0{\cdot}48$. Pulsatile Reynolds number = 0·21, Strouhal number = 0·0031. Hollow dimensions $h = 0{\cdot}05$ cm, $L = 10$, $D = 6$.

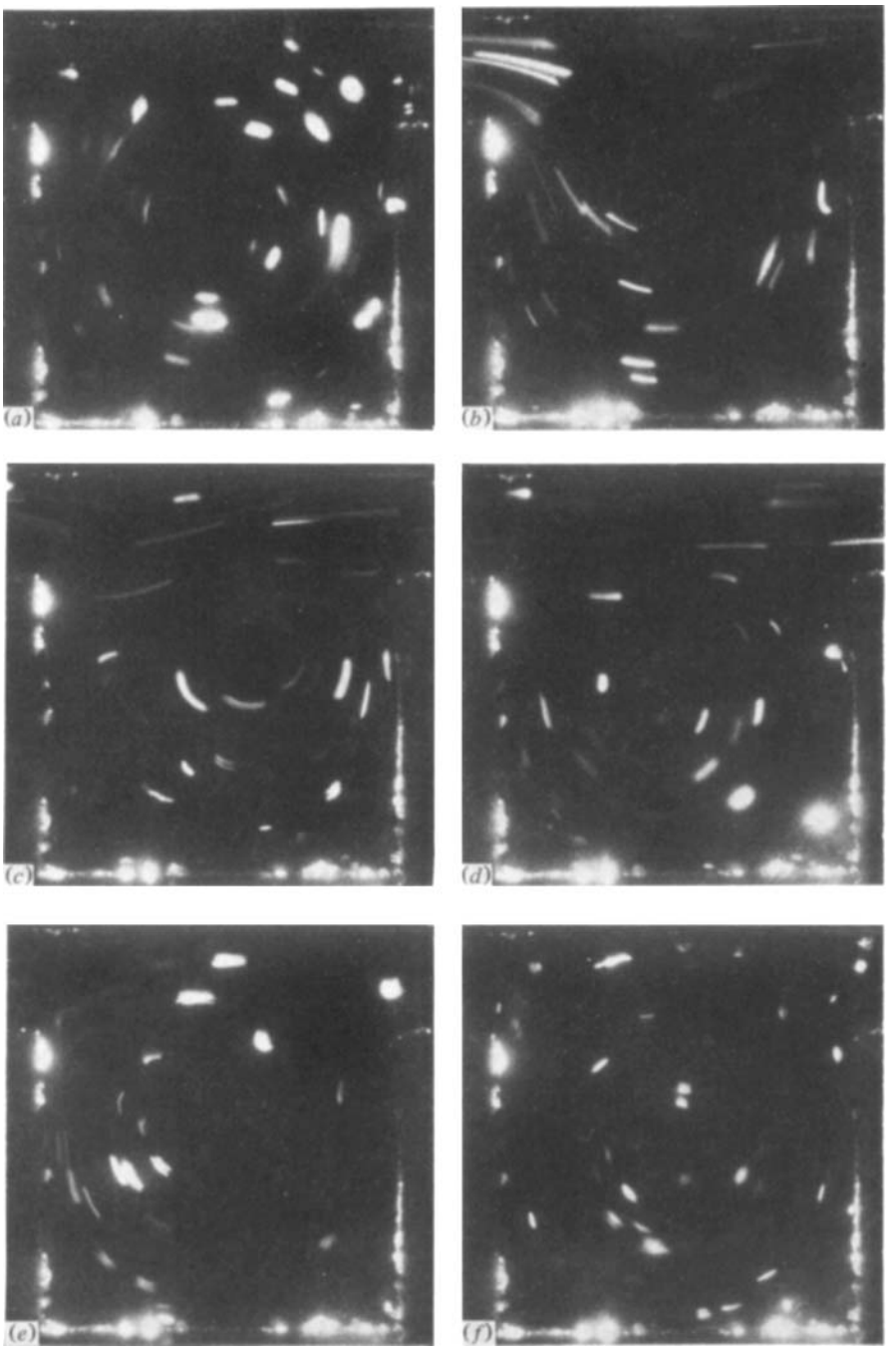

FIGURE 9. Flow cycle for rectangular hollow. (*a*) $t = 0{\cdot}08$; (*b*) $t = 0{\cdot}13$; (*c*) $t = 0{\cdot}19$; (*d*) $t = 0{\cdot}4$; (*e*) $t = 0{\cdot}44$; (*f*) $t = 0{\cdot}57$. Pulsatile Reynolds number 0·21. Strouhal number 0·0031. Hollow dimensions $h = 0{\cdot}05$ cm, $L = 10$, $D = 8$.